Volume 40 | Number 1 | January 2016 | Pages 1–846

NJC

New Journal of Chemistry
www.rsc.org/njc

A journal for new directions in chemistry

ISSN 1144-0546

ROYAL SOCIETY OF CHEMISTRY

PAPER
Jason B. Benedict et al
The role of atropisomers on the photo-reactivity and fatigue of diarylethene-based metal–organic frameworks

CNrs

This is an Accepted Manuscript, which has been through the Royal Society of Chemistry peer review process and has been accepted for publication.

Accepted Manuscripts are published online shortly after acceptance, before technical editing, formatting and proof reading. Using this free service, authors can make their results available to the community, in citable form, before we publish the edited article. We will replace this Accepted Manuscript with the edited and formatted Advance Article as soon as it is available.

You can find more information about Accepted Manuscripts in the **author guidelines**.

Please note that technical editing may introduce minor changes to the text and/or graphics, which may alter content. The journal's standard **Terms & Conditions** and the ethical guidelines, outlined in our **author and reviewer resource centre**, still apply. In no event shall the Royal Society of Chemistry be held responsible for any errors or omissions in this Accepted Manuscript or any consequences arising from the use of any information it contains.

The Effect of Chalcogen Substitution on the Structure and Spectroscopy of 4,7-Dimethyl-2*H*-chromen-2-one/thione Analogues

Zuly Yuliana Delgado Espinosa,[a] Aamer Saeed,[b,*] Shamsul Mahmood,[b] Gustavo A. Echeverría,[c] Oscar E. Piro,[c] Mauricio F. Erben[a,*]

[a] *CEQUINOR (UNLP, CONICET-CCT La Plata), Departamento de Química, Facultad de Ciencias Exactas, Universidad Nacional de La Plata, Bv. 120 e/ 60 y 64 Nº 1465. La Plata (1900), República Argentina.*

[b] *Department of Chemistry, Quaid-I-Azam University, Islamabad 45320, Pakistan.*

[c] *Instituto de Física La Plata, Departamento de Física, Facultad de Ciencias Exactas, Universidad Nacional de La Plata, 49 y 115, La Plata (1900), Buenos Aires, República Argentina.*

* Corresponding authors: (AS) E-mail: aamersaeed@yahoo.com, Tel: +92-51-90642128; Fax: +92-51-90642241. (MFE) E-mail: erben@quimica.unlp.edu.ar, Tel/Fax: +54-211-445-4393.

Abstract

The 4,7-dimethyl-2*H*-chromen-2-one (**1**) and its novel sulfur analogue 4,7-dimethyl-2*H*-chromen-2-thione (**2**) were synthesized and fully characterized by spectroscopic methods and mass spectrometry. The crystal structure of compound **2** has been determined by X-ray diffraction methods and it crystallizes in the monoclinic $I2/m$ space group. The molecular skeleton lies in the crystallographic mirror plane, in agreement with the expected theoretical planarity enforced by extended π-bonding, The crystal packing of both compounds is characterized by $R_2^2(8)$ motif formed by intermolecular C–H$\cdots$X=C (X= O and S) hydrogen-bonding interactions involving the 1-benzopyran-2-one/thione moiety, as also identified by Hirshfeld surfaces analysis. The vibrational properties have been studied by infrared and Raman spectroscopy data complemented by quantum chemical calculations and normal coordinate analysis of the potential energy distribution. The UV-Vis spectrum is interpreted in terms of TD-DFT quantum chemical calculations, showing a clear red-shift in the HOMO-LUMO electronic transition when the chromen-2-one ring is converted in the chromen-2-thione.

Keyword

Coumarin; Thiocoumarin; Vibrational Spectroscopy; Molecular Structure; Substituent Effect

Introduction

Coumarins derivatives, i.e. molecules containing the benzopyran-2-one, or chromen-2-one ring system, are widely distributed throughout nature occurring as secondary metabolites of plant species, notably in the tonka bean and *Melilotus* species.[1] Coumarin was first reported to be synthesized in 1868 by Perkin from salicylahdehyde and acetic anhydride.[2] Since then, the preparation of coumarin and its derivatives has attracted the attention of organic chemists and numerous methods have been developed for their synthesis, the Pechmann condensation and Knowvenagel reactions are widely used.[3]

Coumarin heterocyclic derivatives exhibit diverse biological activities, as reviewed recently.[4] In particular, the anti-cholinesterase activity displayed by coumarin class of compounds have been introduced as anti-Alzheimer´s agents.[5] It has been suggested that the coumarin motif interacts primarily with the pheriperal anionic binding site, preventing the polymerization of β-ambyloid peptide plaques and fibrils formation. Coumarins are also inhibitors of the monoamine oxidase enzyme, a target for treatment of depression and Alzheimer disease.[6] The key role played by coumarines in the pharmacotherapy of breast cancer has been recently reviewed.[7] Lafitte, et al. designed a series of coumarin compounds that inhibit DNA gyrase protein -involved in replication and transcription of bacterial circular DNA- a target for antibacterial agents.[8]

Substitutions on the benzopyrone ring influence the chemical, structural[9] and biological properties of coumarins.[10-12] Moreover, a large degree of structural and chemical diversity is reached by introducing different heteroatoms in the 1- and/or 2- positions of the 1-benzopyran-2-one group. In particular, 2-thiocoumarins are accessible from the corresponding coumarine by using an equimolar amount of p-methoxyphenylthionophosphine sulfide dimer (Lawesson's

Reagent) as sulfur-transfer reagent.[13-15] The simplest 2-thiocoumarin derivative have an essentially planar structure in the solid phase and crystallizes in a non-centrosymmetric space group, being promising candidate for non-linear optical applications, as crystals may display second harmonic generation (SHG) effects.[16] Moreover, analytical applications of thiocoumarins were reported, with significant chromogenic and fluorogenic signaling toward Hg(II) and Au(III) ions, which induce the selective desulfuration of thiocoumarin to coumarin.[17, 18]

Here, the synthesis and characterization of two close species, i.e. 4,7-dimethyl-2*H*-chromen-2-one (also known as 7-methyl-4-methyl-coumarin) (**1**),[19] and 4,7-dimethyl-2*H*-chromen-2-thione (also known as 7-methyl-4-methyl-thiocoumarin) (**2**) (see Scheme 1) is presented. The aim of this work is to provide a structural and spectroscopic study for these molecules and analyse the influence of the heteroatom in the 2-one/thione group. Thus, the analysis of the X-ray molecular structures and vibrational FTIR and FT-Raman spectra is presented and analysed with the help of a normal mode coordinate analysis and quantum chemical calculations at the B3LYP/6-311++G(d,p) level of approximation. Furthermore, the electronic spectra for both compounds have been determined and analysed in terms of TD-DFT methods and results from the Natural Bond Orbital (NBO)[20] population analysis.

Scheme 1. 4,7-dimethyl-2*H*-chromen-2-one/thione derivatives


X= O (**1**) and S (**2**)
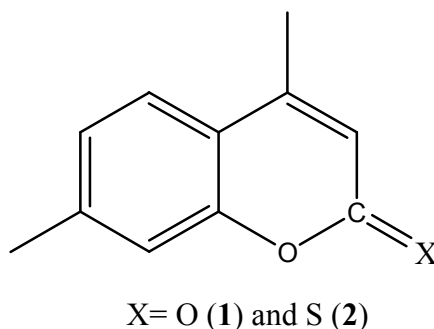
2-Experimental

2.1-Synthesis. Preparation of substituted 4-methyl coumarin was achieved by placing 2 g (0.0185 mole) of pure 3-methyl phenol in a 250 ml round bottom flask and adding 1.77 ml of ethyl acetoacetate and mixing to get a clear solution. This solution was cooled to 5-10 °C. Meanwhile, 10 ml of concentrated H_2SO_4 was cooled to about 5-10 °C in an ice bath. The above solution was added drop by drop into concentrated H_2SO_4 with vigorous stirring.[19] The resultant dark green solution was cooled and was stirred into crushed ice. The solid product thus separated out, was allowed to settle down. Crude product was filtered off, repeatedly washed with water and recrystallized from ethanol to get crystals.

Thionation of compound **1** with Lawesson reagent (LR) was conducted as described in the literature for similar coumarines.[13, 21, 22] The standard procedure uses 3 mmol of compound **1** in 3 mL of toluene with 3 mmol of LR, the resulting mixture was refluxed during 3.5 h with stirring, cooled to ambient temperature and then concentrated in vacuum to yield a yellow solid. It was further recrystallized from ethanol/water (1/1) and slow evaporation yields small crystals suitable for X-ray analysis.

Scheme 2. Synthetic route for compounds 1 and 2.
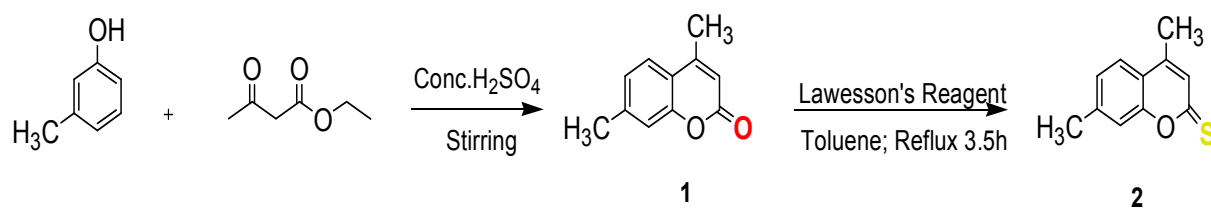
4,7-Dimethyl-2H-chromen-2-one (1): Yield 75%, mp 131°C; R*f*: 0.40 (Petroleum ether: ethyl acetate 4:1); IR (KBr pellets, cm^{-1}): 1702-1706 (C=O), 1619, 1583-1586 (Ar-C=C); ^{1}H NMR (DMSO, 300 MHz) δ: 7.29-6.71 (m, 3H, Ar-H), 4.17 (s, 1H, C-H), 2.31 (s, 3H, C-H), 2.10 (s, 3H, C-H); ^{13}C NMR (75 MHz) δ (ppm): 160.4 (C=O), 151.2 (C=C), 150.1 (Ar), 136.0 (Ar), 125.7 (Ar), 124.4 (Ar), 120.6 (Ar), 119.8 (Ar), 113.4 (Ar), 24.6 (C-H), 20.5 (C-H); GC-MS (m/z): 174 ([M]$^+$,68%); 146 ([C$_{10}$H$_{10}$O]$^+$, 100%); 131 ([C$_9$H$_7$O]$^+$, 27%); 115 ([C$_9$H$_7$]$^+$, 33%).

4,7-Dimethyl-2H-chromen-2-thione (2): 94% Yield, mp 118 °C; IR (KBr pellets, cm^{-1}): 1623-1530 (Ar C=C), 1300 (vs), 1169 (s), 1112 (s); ^{1}H NMR (CDCl$_3$, 200 MHz) δ: 7.59-7.59 (m, 3H, Ar-H), 7.18 (s, 1H, C-H), 2.51 (s, 3H, C-H), 2.41 (s, 3H, C-H); ^{13}C NMR (200 MHz) δ: 197.5(C=S), 156.3, 144.5, 143.5, 128.2, 126.6, 124.2, 119.2, 117.2, 21.8, 18.0; GC-MS (m/z): 190 ([M]$^+$,72%); 146 ([C$_{10}$H$_{10}$O]$^+$, 100%); 131 ([C$_9$H$_7$O]$^+$, 15%); 115 ([C$_9$H$_7$]$^+$, 21%).

2.2-Instrumentation. Melting point was determined using a digital Gallenkamp (SANYO) model MPDBM 3.5 apparatus and is uncorrected. ^{1}H NMR and ^{13}C NMR spectra were determined in CDCl$_3$ with a 300 MHz Bruker AM-300 spectrophotometer. The GC-MS measurements were recorded with a GCMS-QP2010 SHIMADZU instrument using gaseous helium as mobile phase with the pressure in the column head equal to 100 kPa. The column used was a 19091J-433 HP-5 (30 mm x 0.32 mm x 0.25 mm). 1 µL volume of the compounds dissolved in CHCl$_3$ and C$_2$H$_5$OC(O)CH$_3$ were chromatographed using the following general conditions: the injection temperature was 200 °C, the initial column temperature (70 °C) was kept for 2 min, then the temperature was increased to 200 °C (heating rate of 10 °C/min) and maintained at this temperature for 4 min. This was followed by a final heating to 250 °C (10 °C/min) after which the column was kept at this temperature for further 2 min. The spectrometer source temperature was maintained at 200 °C. Elemental analyses were conducted using a LECO-183 CHNS analyzer.

2.3-Crystal structure determination. The measurements were performed on an Oxford Xcalibur, Eos, Gemini CCD difractometer with graphite-monochromated CuKα (λ = 1.54184 Å) radiation. X-ray diffraction intensities were collected (ω scans with ϑ and κ-offsets), integrated and scaled with CrysAlisPro suite of programs.[23] The unit-cell parameters were obtained by least-squares refinement (based on the angular settings for all collected reflections with intensities larger than seven times the standard deviation of measurement errors) using CrysAlisPro. Data were corrected empirically for absorption employing the multi-scan method implemented in CrysAlisPro.

The possible space groups and crystal structure were determined by the intrinsic phasing procedure implemented in SHELXT of the SHELX suit of programs,[24] assuming as prior information a primitive cell (*P*), the Laue group (2/*m*), and the presence of the expected non-H atomic species in the solid, namely S, O, and C. There were selected six space groups having the best figure of merit out of the 8 centrosymmetric and 6 non-centrosymmetric ones evaluated, namely the center-symmetric P2$_1$/c and P2/m and their respective non center-symmetric subgroups P2$_1$ and Pc, and P2 and Pm. We disregard all these subgroups as the center-symmetric test of intrinsic phasing clearly indicated the inversion-related character of the atoms constellation (quantified by the small phase error α_0= 0.065) and the absolute structure Flack parameter x was close to 0.5 hence indicating a racemic mixture. The structure in both *P*2$_1$/*c* and *P*2/*m* space groups easily yielded to intrinsic phasing which lead to a single independent molecule showing pseudo-mirror symmetry [*rms* deviation of non-H atoms from the best least-squares plane of 0.0047 Å] in P2$_1$/c, and to two independent molecules at special positions of mirror-symmetry in *P*2/*m* group. In these space groups, the atomic species assigned from the integrated electron density around the peaks of the map determined the correct non-H chemical formula, namely C$_{11}$OS. At this stage, it

turned out more appropriated to describe the solid by the *I*2/*m* space group. In fact, in this group there is a single molecule per asymmetric unit laying on a crystallographic *m*-plane, as theoretically expected for a planar molecule.

The molecular model was refined by full-matrix least-squares with SHELXL of the SHELX package. All H-atoms were located in a Fourier difference map phased on the heavier atoms and refined at their found positions with isotropic displacement parameters and C–H bond distances restrained to a target value of 0.96(1) Å. Crystal data, data collection procedure, and refinement results are summarized in Table 1. Crystallographic structural data have been deposited at the Cambridge Crystallographic Data Centre (CCDC). Enquiries for data can be direct to: Cambridge Crystallographic Data Centre, 12 Union Road, Cambridge, UK, CB2 1EZ or (e-mail) deposit@ccdc.cam.ac.uk or (fax) +44 (0) 1223 336033. Any request to the Cambridge Crystallographic Data Centre for this material should quote the full literature citation and the reference number CCDC 1540188. Crystal data, structure refinements and geometrical parameters are given as Electronic Supplementary Information (ESI, Tables S1-S4).

2.4- Spectroscopy. Solid-phase (in KBr pellets) infrared spectra were recorded with a resolution of 2 cm^{-1} in the 4000-400 cm^{-1} range on a Bruker EQUINOX55 FTIR spectrometer. Raman spectra for compounds **1** and **2** in the solid phase were recorded using a Horiba Jobin Yvon T64000 Raman spectrometer equipped with a liquid N_2-cooled back-thinned CCD detector. Spectra were recorded as the co-addition of up to 16 individual spectra with CCD exposure times of 10-20s each. Compound **1** was powdered and mixed with K_2SO_4 for diminishing the fluorecence signal. UV-Vis spectra in Dichloromethane solution were recorded using a standard quartz cell placed in the sample compartment of a Shimadzu Model 2600/2700 spectrometer (2 nm resolution).

2.5- Computational details. Molecular quantum chemical calculations have been performed with the GAUSSIAN 03 program package [25] by using the B3LYP DFT hybrid methods employing Pople-type basis set.[26] The valence triple-ξ basis set augmented with diffuse and polarization functions in both the hydrogen and weighty atoms [6-311++G(d,p)] has been used for geometry optimization and frequency calculations. The calculated vibrational properties corresponded in all cases to potential energy minima for which no imaginary frequency was found. The Potential Energy Distribution PED analysis are computed from the B3LYP/6-311++G(d,p) calculated vibrational frequencies using VEDA4 program.[27, 28] Natural population analysis and second-order Donor$\rightarrow$ acceptor interaction energies were estimated at the B3LYP/6-311++G(d,p) level by using the NBO analysis.[20] The vertical transition energies were calculated at the optimized ground-state geometry using the time-dependent density functional theory [29] at the same level of theory used for optimization an vibrational calculations taking into account solvent effects (CH_2Cl_2) through the Polarizable Continuum Model [30] to produce a number of 10 singlet-to-singlet transitions.
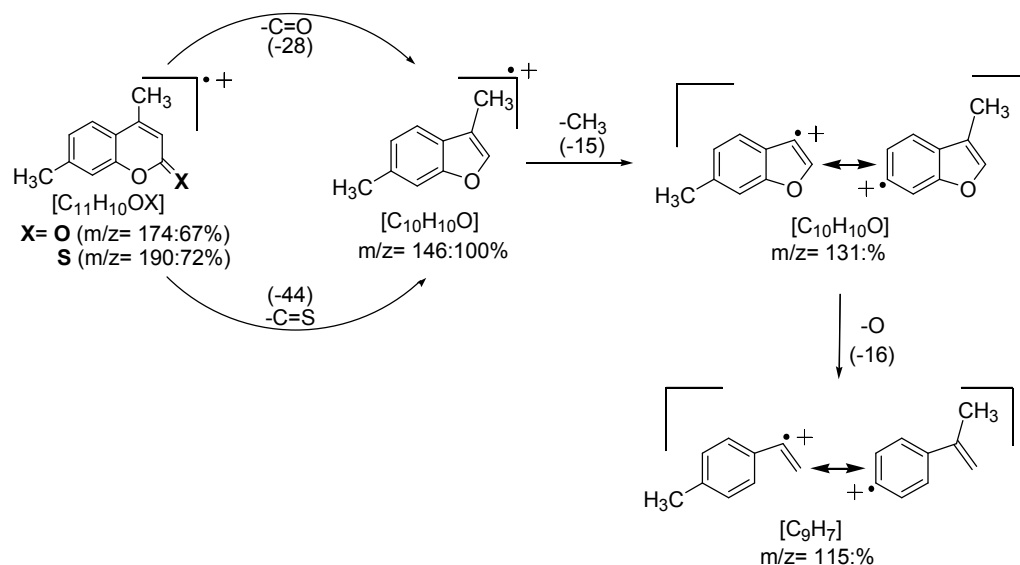
2.6- Hirshfeld surface analysis. Hirshfeld surfaces and their associated two-dimensional fingerprint plots [31-34] are plotted using CrystalExplorer 3.1 software.[35] The normalized contact distance *(d*$_{norm}$) surface and the breakdown of two-dimensional fingerprint plots are used for decoding and quantifying intermolecular interactions in the crystal lattice. 3D d_{norm} surfaces are mapped over a fixed color scale of -0.08 au (red) – 0.6 Å au (blue), *Shape index* mapped in the color range of -1.0 au (concave) -1.0 au (convex) Å, and *Curvedness* in the range of -4.0 au (flat) $- 0.01$ au (singular) Å. The 2D fingerprint plot displayed by using the translated 0.6–2.6 Å range, and including reciprocal contacts.

3- Results and Discussion

3.1- Electron impact ionization

The fragmentation of coumarin under electron ionization (EI) conditions was early described by Porter.[36] Under EI conditions, its mass spectrum exhibits an abundant molecular ion and also abundant fragment ions attributed to loss of CO from the pyrone ring to form the benzofuran radical ion. This fragmentation pathway was elegantly verified by Kutney et al. [2] using high-resolution mass spectrometry for a series of coumarins.[37] Less known, however, is the behaviour of the corresponding thio analogue under electron impact ionization. Compounds **1** and **2** were analyzed by gas chromatography and mass spectrometry (see Figures S1 and S2 in the ESI material). The fragmentation pattern of both compounds is very similar, the molecular ion being clearly observed at m/z= 174 and 190, for compounds **1** and **2**, respectively. Major observations on the fragmentation under EI condictions include the elimination of CO or CS to give the same benzofuran "odd electron" ion at m/z= 146, being the most abundant ion detected for both compounds. The mass spectra show the loss of a methyl group for this ion which results in the ion at m/z= 131, also found for **1** and **2**. The loss of a oxygen from the benzofuran ring generates the ion at m/z= 115 observed in both mass spectra.

Scheme 3. Electron ionization fragmentation of compounds **1** and **2**.

3.2- Structural analysis and Hirshfeld surface analysis

An ORTEP [38] view of the $S_{11}H_{10}OS$ molecule is shown in Figure 1 where it is compared with the closely related $C_{11}H_{10}O_2$ molecule. The corresponding molecular bond distances and angles are included in Table 2, together with the computed geometrical parameters [6-311++G(d,p)].

The 1-benzopyran-2-one ring in compound **1** is essentially planar (the *rms* deviation of non-H atoms from the best least-squares plane is 0.009 Å), in agreement with the structure reported in similar molecules,[39, 40] while compound **2** is described by the *I*2/*m* space group, the molecule laying on a crystallographic *m*-plane, as theoretically expected for a planar molecule. Geometrical parameters are similar for both molecules. The C1–O bond length is slightly longer for the oxygen analogue [1.378(2) Å], as compared with the value of 1.361(3) Å determined for compound **2**. The bond angles around the O-C=X group show little variation with the chalcogen substitution, with O–C=X and C–C=X (X= O/S) values of 116.6 (1)°/ 117.6 (2)° and 126.2(1)° /125.3(2)°, respectively. The agreement between the computed and experimental geometrical parameters is very good. The

mean average deviation between the B3LYP/6–311++G(d,p) and experimental bond lengths and bond angles are 0.004/0.009 Å and 0.08/0.003°, with a maximum error of 0.017/0.022 Å and 1.1/0.9°, for the C1O1/C2C3 bond length and O1C1C2/C3C4C5 angle, for compounds **1** and **2,** respectively.

Table 1. Crystal data and structure refinement results for compound **2**.

| Parameter	Compound 2
Empirical formula	$C_{11}H_{10}OS$
Formula weight	190.25
Temperature/K	293(2)
Crystal system	Monoclinic
Space group	I 2/m
a/Å	11.0492(8)
b/Å	6.9453(6)
c/Å	13.528(1)
α/°	
β/°	107.219(8)
γ/°	
Volume/Å^3	991.57(14)
Z	4
Density/cm^3	1.274
Absorption coefficient /mm^{-1}	2.529
F(000)	400
Crystal size/mm^3	-
Radiation	-
2Θ range for data collection/°	4.558 to 72.342°.
Index ranges	$-13 \leq h \leq 13$, $-8 \leq k \leq 7$, $-15 \leq l \leq 16$
Reflections collected	3025
Independent reflections	1049 [R(int) = 0.0184]
Data/restraints/parameters	1049 / 9 / 105
Goodness-of-fit on F^2	1.039
Final R indexes [I>=2σ (I)]	R1 = 0.0495, wR2 = 0.1350
Final R indexes [all data]	R1 = 0.0596, wR2 = 0.1507
Largest diff. peak/hole / e Å^{-3}	0.142 and -0.230 e.Å^{-3}
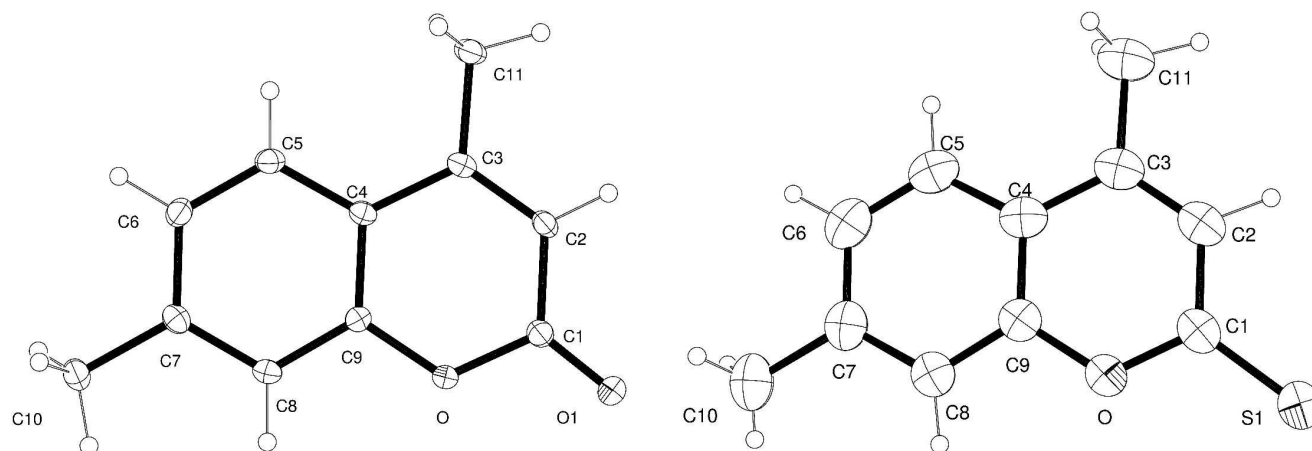
Figure 1. Drawings of 4,7-dimethyl-2*H*-chromen-2-one[19] (**1**, left) and 4,7-dimethyl-2*H*-chromen-2-thione (**2**, right) molecules showing the numbering of the non-H atoms and their displacement ellipsoids at the 30% probability level.

Table 2. Selected geometric parameters of 4,7-dimethyl-2H-chromen-2-one (**1**) and 4,7-dimethyl-2H-chromen-2-thione (**2**).

Bond distance (Å)	Compound 1 [19]		Compound 2		Bond Angle (°)	Compound 1 [19]		Compound 2	
	Calc	Exp.	Calc	Exp.		Calc	Exp.	Calc	Exp.
O1-C2	1.395	1.378(2)	1.371	1.361(3)	C2-O1-C9	122.3	121.6(1)	122.5	121.8(2)
O1-C9	1.363	1.379(2)	1.366	1.377(4)	O1-C2-C3	116.0	117.2(1)	116.6	117.1(3)
C2-C3	1.453	1.445(2)	1.437	1.43(3)	O1-C2-X11	117.7	116.6(1)	118.2	117.6(2)
C2-X11	1.204	1.211(2)	1.651	1.634(4)	C3-C2-X11	126.3	126.2(1)	125.2	125.3(2)
C3-C4	1.355	1.345(2)	1.361	1.339(4)	O1-C9-C10	121.8	121.1(1)	121.6	121.2(3)
C4-C12	1.503	1.500(2)	1.502	1.503(4)	O1-C9-C8	116.0	116.3(1)	116.4	115.7(2)
C4-C10	1.452	1.450(2)	1.449	1.445(4)	C3-C4-C12	121.1	121.1(1)	121.2	121.2(2)
C5-C6	1.383	1.375(2)	1.383	1.367(4)	C3-C4-C10	118.6	118.7(1)	118.3	118.7(2)
C5-C10	1.408	1.404(2)	1.408	1.400(5)	C12-C4-C10	120.3	120.3(1)	120.5	120.0(3)
C6-C7	1.408	1.405(2)	1.408	1.398(5)	C4-C10-C9	118.1	118.5(1)	117.8	118.0(3)
C7-C8	1.391	1.385(2)	1.391	1.378(4)	C4-C10-C5	124.6	124.8(1)	125.0	125.9(2)
C7-C13	1.508	1.506(2)	1.508	1.506(5)	C5-C10-C9	117.3	116.7(1)	117.2	118.0(3)
C8-C9	1.395	1.386(2)	1.394	1.382(4)					
C9-C10	1.404	1.399(2)	1.404	1.391(3)					

In the crystal packing, molecules of **1** are linked forming one-dimensional chains *via* C2–H⋯O=C hydrogen bonds (dH⋯O = 2.50 Å) of a $R_2^2(8)$ motif [symmetry code: -x, 1-y, 1-z], as shown in Figure 2. The corresponding pairs of mean planes are close to parallel-displaced to each other and chains arrange in 2-D nearly planar sheets involving centrosymmetric dimers interconected by H⋯O hydrogen bonds [symmetry code: 1-x, 2-y, 1-z]. The 7-CH$_3$ and C=O groups (dH⋯O = 2.61 Å) interacts in a tail-to-head manner adopting a $R_2^2(16)$ moiety. The 3-D network is further completed by weaker CH$_3$⋯O=C interactions (dH⋯O = 2.71 Å) involving the 4-CH$_3$ group [symmetry code: x, 1+y, z] (See Figure 2, botton).

The compound **2** interacts via two centrosymmetric dimers forming sheets in a perfectly plannar arrangemet. Similar to compound **1**, the C2–H group in the benzopyrone ring interacts with the S=C bond [symmetry code: 2-x,y,-z] forming a $R_2^2(8)$ motif (dH⋯S = 2.87 Å), as shown in Figure 2. The C8–H group also acts as a donor forming centrosymmetric dimers helds by C8–H⋯S=C hydrogen bond (dH⋯S = 2.96 Å) [symmetry code: -x+1,+y,-z] forming a $R_2^2(12)$ motif.
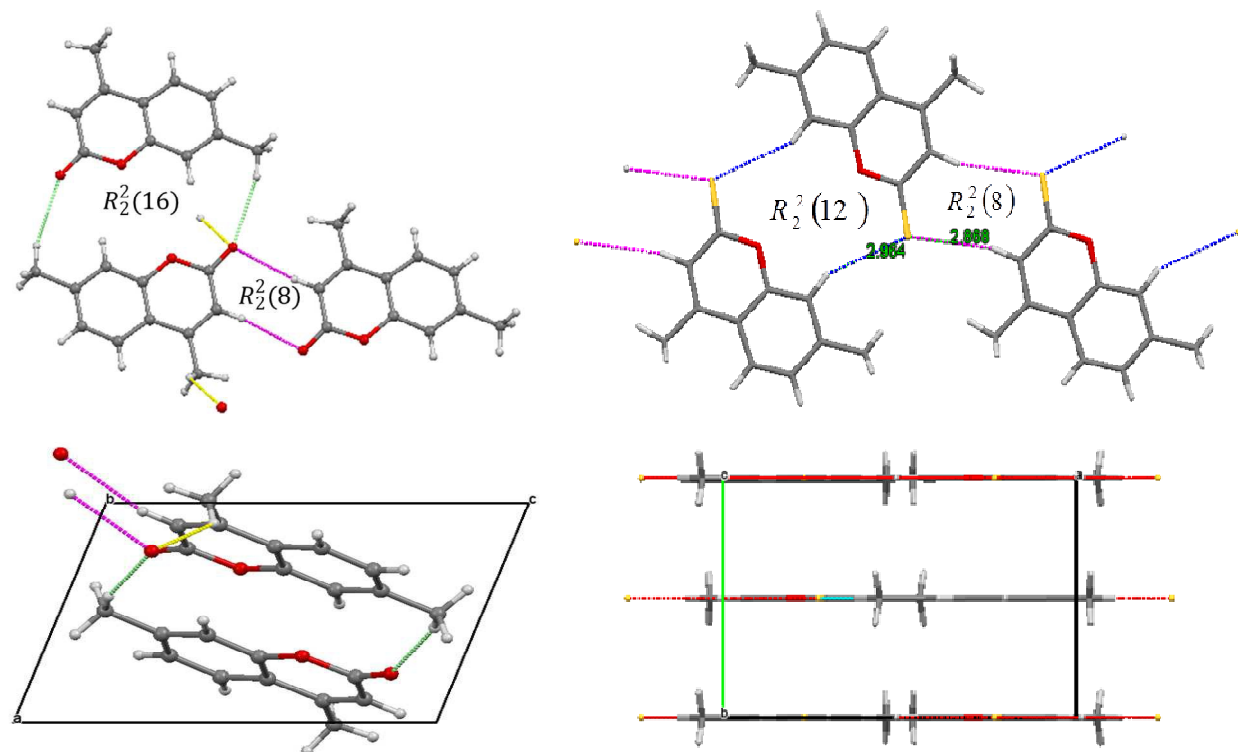
Figure 2. Top panel: packing diagram of compounds **1** [19] and **2** showing $R_2^2(8)$ motif *via* intermolecular C2–H•••S hydrogen bonds and C8–H•••S interactions for 2 forming $R_2^2(12)$ motif. Botton panel:*b*- and *c*-axis view of the hydrogen-bonding interactions in **1** and **2,** respectively.

Following Seth et al. [19] the Hirshfeld surfaces and the associated 2D fingerprint plot were calculated to better understand the role of non-classic hydrogen bonds interactions in the crystal packing of the title compounds. Figure 3 shows surfaces mapped over the d_{norm}, shape index and curvedness properties for compounds **1** and **2**. For **1**, the C–H···O hydrogen bond involving the C2–H donor can be clearly recognized by the red regions around the chromen-2-one group. A close examination with Shape index and Curvedness Hirshfeld surface properties has been done to identify planar stacking arrangements.[32] π-π stacking of six-membered rings are usually characterizaed by a typical pattern of touching red and blue triangles on the shape index surface

(Fig. 4, column 2).[34] The red triangles are concave regions associated with atoms of the π-π stacked rings above them, while the blue triangles are convex regions indicating the aromatic ring atoms of the molecule inside the surface. For compounds **1** and **2**, the red triangles clearly observed in the centers of the benzopyrone ring complemented with touching blue triangles over C4, C6 and C8 depicts the presence of C···C contacts indicating π-stacking interactions. These are characterized by intercentroid distances $Cg1···Cg2$ = 3.5500(8) Å (symmetry code: 1-x,1-y,1-z), and 3.5341(3) Å (symmetry code: 3/2-x,1/2+y,1/2-z), respectively (see Figure S3 in the ESI section). This features are in excellent agreement with the recent Hirshfeld study of coumarin derivatives reported recently by Malecka and Budzisz.[41]

Figure 3. Hirshfeld d_{norm}, Shape index and Curvedness surfaces for molecules **1** and **2**.
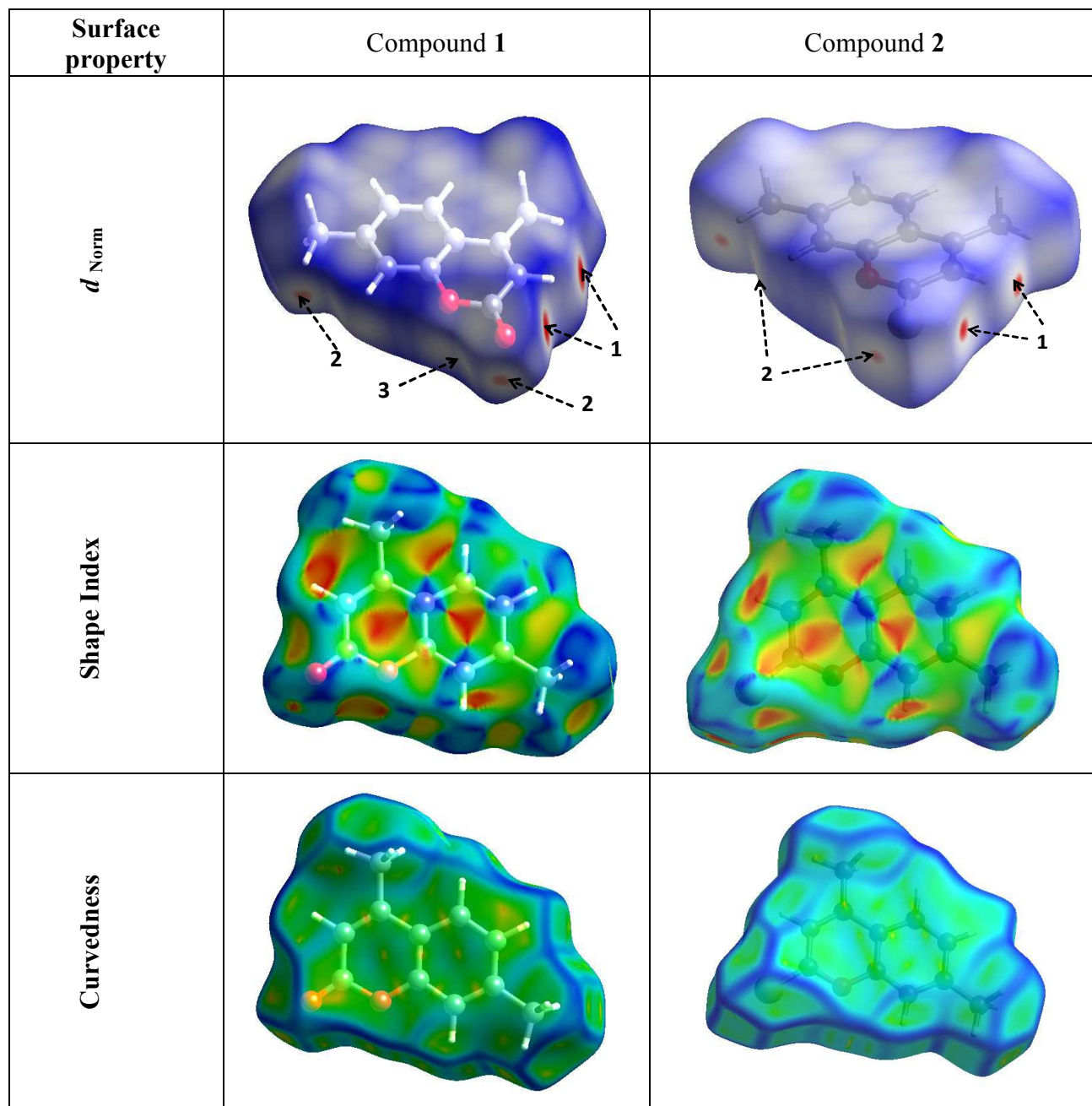
The relative contributions to the Hirshfeld surface area due to main intermolecular contacts for the compounds **1** and **2** are shown Figure 4. These fingerprint plots show that the methyl substituents on the ring play a key role in the participation of each type of contact. For both structures the H···H interactions (labeled 1) have the highest contribution witn 48.9% and

44.7%, respectively. The pairs of narrow pointed spikes in compounds **1** (labelled 2) and **2** (labelled 6) show the presence of H⋯O and H⋯S contacts with contribution of 27.3% and 21.4% respectively. These contacts are forming the dimers in crystal packing through C-H…(X) hydrogen bonds. The π-π stacking (C⋯C) contacts are shown (labelled 4) on the diagonal at around (de + di) = 1.8 Å, these interactions comprise 12.6% for **1** and 12.5% for **2**.

Figure 4. Fingerprint plots for compounds **1** (left) and **2** (right). Close contacts are labelled as: (1) H⋯H, (2) O⋯H, (3) C⋯H, (4) C⋯C, (5) O⋯C, (6) S⋯H and relative contributions of intermolecular contacts to the Hirshfeld surface area.
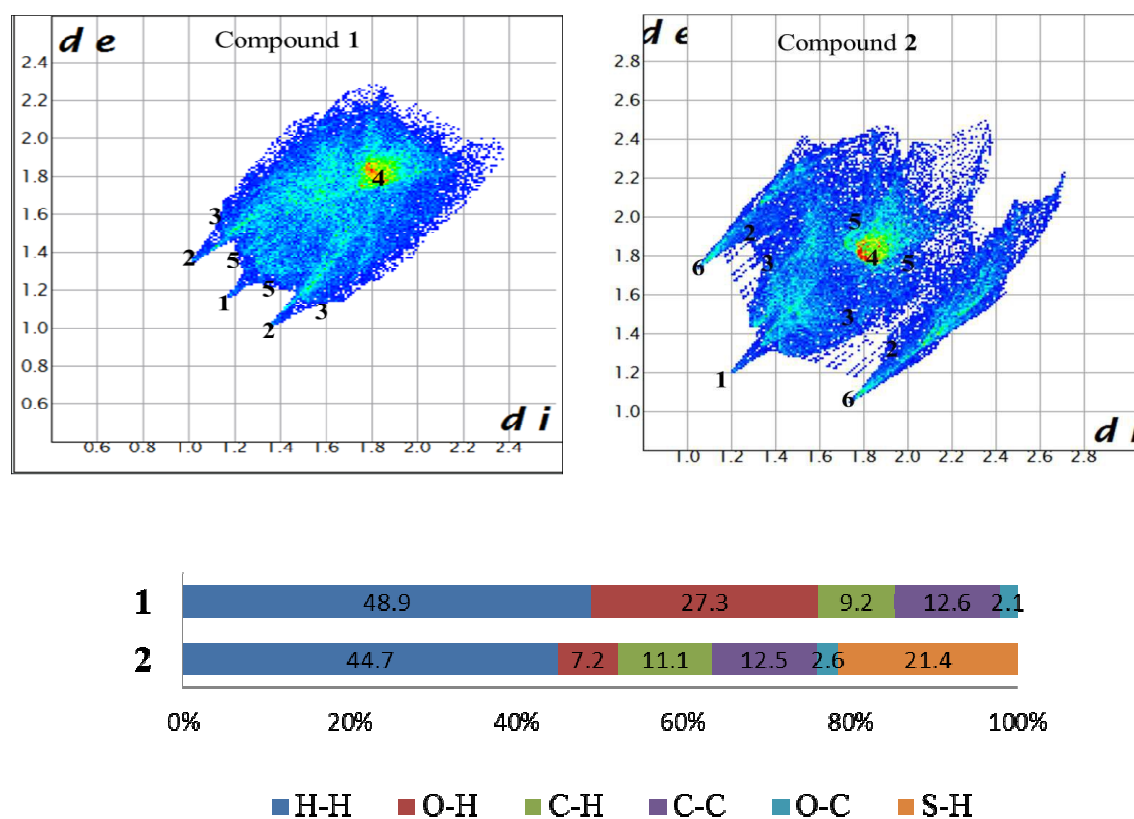
3.3-Vibrational properties

Figures 5 and 6 show the solid state infrared and Raman spectra of compounds **1** and **2**, respectively. The observed and calculated infrared absorptions, the FT-Raman frequencies along with their relative intensities and assignments are summarized in Tables 3 and 4 for **1** and **2**, respectively. The 3N–6 = 63 normal modes of vibration can be classified as 41 A′ in-plane modes and 22 A″ out-of-plane modes in the C_S symmetry group computed for the vaccum isolated molecule. The assignment of the bands was determined from the normal coordinate analysis aided by visualization of the animations for displacement vectors of localized vibrational modes and complemented by comparison with spectra of related molecules.[42-45] The joint analysis of the infrared and Raman spectra allows for a complete description of the vibrational properties of compounds **1** and **2**, which is in good agreement with the harmonic frequencies obtained with the B3LYP/6-311++G(d,p) level of calculations.

For compound **1**, the most salient features are the νC=O and νC1–O stretching modes, appearing as intense absorptions at 1717 (1698 cm^{-1} in Raman) and 1149 cm^{-1} (1148 cm^{-1} in Raman), respectively, in good agreement with the values reported for related species.[46] The computed values are 1798 and 1151 cm^{-1}, suggesting that the relatively low frequency value experimentally observed for the νC=O is related with intermolecular interactions involving the carbonyl group in the crystalline compound **1**.

A strong absorption is also observed at 1619 cm^{-1} in the infrared spectrum of compound **1**, with a counterpart at 1614 cm^{-1} in the Raman spectrum. According to the potential energy distribution analysis, this mode is assigned with confidence to a pure νC=C stretching mode of the coumarin system, also in agreemet with the quantum calculations, which predicts the occurrence

of the most intense νC=C mode at 1654 cm^{-1} with the expected a' symmetry. The analysis of the

Raman spectra allows for a clear assignment of the C-C stretching modes in the benzopyrone ring,
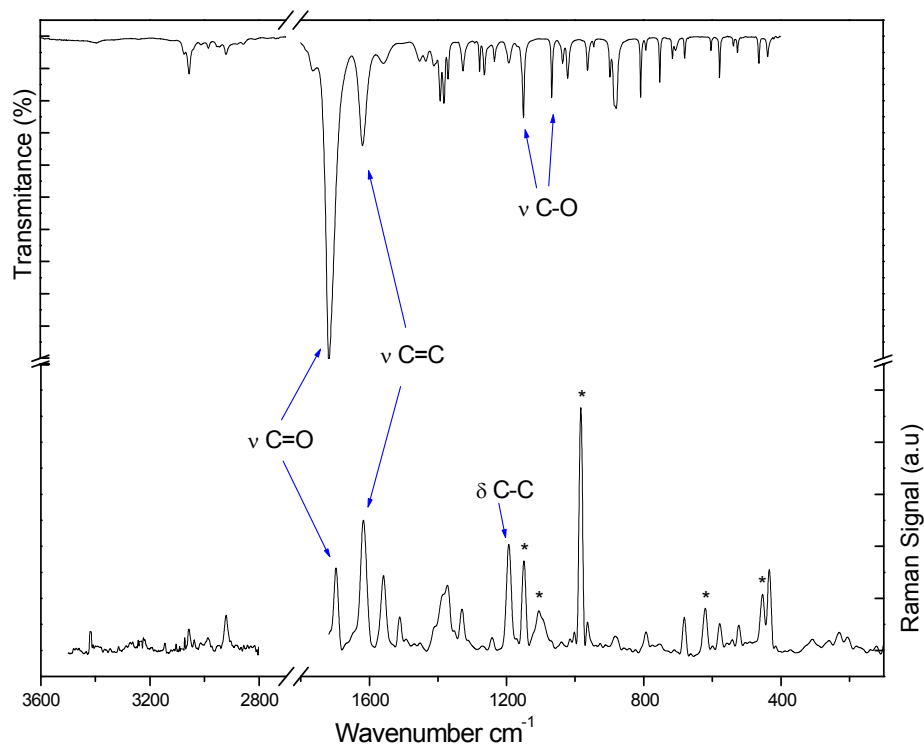
with signals at 1559, 1512 and 1412 cm^{-1}.[14, 45]

Figure 5. FT-Raman and FTIR spectra for compound **1** in the solid phase (bands in the Raman

spectrum marked with * correspond to K$_2$SO$_4$).

Table 3. FTIR and Raman experimental data for compound **1**, together with the computed

B3LYP/6-311++G(d,p) values and tentative normal mode assignment

Experimental		Calculated [b]	Assignment [c] / % PED
IR [a]	Raman		
3073$_m$	3082$_w$	3200 (1)	a'/ν CH (99)
3055$_m$		3193(7)	a'/ ν CH (100)
3011$_w$		3190(4)	a'/ CH (90)
3984$_w$		3167(8)	a'/ ν CH (100)
		3121(16)	a' / ν_{as} CH$_3$-Py (85)

2919_m	2921_m	3110(14)	a' / ν_{as} CH_3-Ph (82)
		3079(9)	a''/ν_{as} CH_3-Py (100)
		3076(13)	a''/ν_{as} CH_3-Ph (100)
		3030(11)	a'/ ν_s CH_3-Py (99)
		3027(25)	a' / ν_s CH_3-Ph (100)
$1763_{s,sh}$; 1717_{vs}	1698vs	1798(776)	ν C=O (82)
		1661(36)	a' / ν CC (100)
1619_{vs}	1614_{vs}	1654(184)	a' / ν CC ring Ph (95)
1560_s	1559_s	1583(35)	a' / ν CC ring Py (21); ν CC ring Ph (79)
	1512_w	1535(4)	a' / δ CC (77); δ CH (32)
		1495(30)	a' / δ_{as} CH_3-Ph (61); δ_{as} CH_3-Py (39)
		1490(5)	a' / δ_{as} CH_3-Py (67); δ_{as} CH_3-Ph (33)
		1486(8)	a'' / δ_{as} CH_3-Ph (79); τ C_6-C_7-C_{13}-H (16)
		1482(10)	a'' / δ_{as} CH_3-Py (80); τ C_3-C_4-C_{12}-H (15)
1411_w	1412_{sh}	1438(18)	a' / ν CC ring Ph (56) ; δ CH (44)
		1418(34)	a' / δ_s CH_3-Py (68); δ CH (32)
		1414(1)	a' / δ_s CH_3-Ph (93)
		1397(39)	a' / δ_{as} C_3-C_4-C_{10} (50); δ CH (27); δ_s CH_3-py (23)
	1328_w	1360(19)	a' / δ CC ring Ph (99)
		1298(7)	a' / δ HCC ring Ph (85); ν CC (15)
		1282(20)	a' / Ph- ring breathing
	1237_w	1246(10)	a' / δ CCH Py (90)
	1194_s	1195(7)	a' / δ CH Ph (58)
		1175(17)	a' / δ CH ring Ph (64); ν CC (36)
1149_s	1148_w	1151(63)	a' / ν_{as} COC (34); ν OCC (34); δ CH ring Ph (32)
1066_s		1077(24)	a' / Ph-Py ring breathing
		1060(<1)	a'' / ρ CH_3-Py (20) ; τ C_{10}-C_4-CH_3 (50); γ C_{12}-C_{10}-C_4-C_3 (13)
1036_m		1058(6)	a'' / ρ CH_3-Ph (25) ; τ C_{10}-C_4-CH_3 (60); γ C_{13}-C_8-C_7-C_6 (16)
1019_m		1035(44)	a' / ν C_7-C_8 (21); δ C_7-C_6- C_5 (23); τ H-C_{13}-C_7-C_6 (54)
		1022(4)	a' / τ H-C_{12}-C_4-C_{10}(57); τ H-C_{13}-C_7-C_6 (43)
961_m	974_w	973(18)	a' / δ CC ring Ph (44); ν CC (20); δ CH3-Ph (20); ν_{as} COC (16)
	958_w	965(1)	a'' / ρ H-C_6-C_7-H (43); ρ H-C_6-C_7-C_{13} (44)
896_m		888(2)	a'' / ρ H-C_8-C_7-C_{13} (82); γ O-C_8-C_9-C_{10} (13)
883_s	881_m	878(44)	a'' / ρ C_8-C_7-C_{13} (14); τ H-C_{11}-C_{12}-O (72); γ O-C_2-O-C_3 (13)
878_s		872(45)	a' / δ CO (69)
807_s		820(21)	a'' /ρ H-C_5-C_6-H (42); τ H-C_6-C_7-C_{13} (57)
792_w	795_m	800(1)	a' / ν C_{13}-C_7 (11); δ C-O-C(15); Ph- ring breathing (74)
750_w	747_s	749(5)	a'' / τ C_4-C_{10} (30);τ C_8-C_9 (26); γ O-C-O-C (43)
714_m		712(3)	a' / δ ring Ph (53); ν CC (32)
705_m		710(4)	a'' / τ H-C_3-C_2-O (33); γ OCOC (67)
679_m	680_m	688(3)	a' / δ ring Ph (75); δ COC (23)
602_m	616_m	603(3)	a'' / τ C_5-C_6-C_7-C_8 (32); γ C-CH_3 (68)
576_s	578_m	579(8)	a' / δ OCO (27); δ CC (13)
535_m		543(2)	a'' / τ H-C_{12}-C_4-C_{10} (17); γ O-C_9-C_8-C10 (43)
524_w	522_m	528(1)	a' / δ ring Py (43); δ COC (23)
463_m	454_s	465(8)	a' / δ ring Ph (73)
438_m	429_w	448(9)	a'' / τ C-C ring Ph (75); γ C_6-C_7-C_8-C_{13} (24)
		431(1)	a' / δ COC (51); δ CC (28)
		374(1)	a' / δ CH_3-Ph (58); δ OCO(17)
	307_m	307(1)	a' / ρ CH_3- Py (77); ρ CH_3-Ph (23)
	260_m	275(<1)	τ CCCC (20); γ OCCC (12)
	228_m	247(<1)	a'' / γ $C_4C_{10}C_5C_9$ (56); γ $C_3C_4C_{10}C_{12}$ (16); τ $C_5C_6C_7C_8$ (27)
		220(1)	a' / δCC (43); δ O-C_9-C_8 (16)
	204_m	205(2)	a'' / τ H-C_{12}-C_4-C_{10} (68); τ C_3-C_4-C_{10}-C_9 (32)
	171_w	167(<1)	a'' / τ C3-C4-C10-C9 (51); γ C-CH3 Py(29)
	117_w	100(<1)	a'' / τ C_2-O-C_9-C_8(43); τ C_6-C_7-C_8-C_9 (24); γ OC_{10}-C_8-C_9 (23)

89(2)	a" / τ C$_2$-O-C$_9$-C$_{10}$ (46); τ C$_7$-C$_8$-C$_9$-C$_{10}$ (35); τ C$_5$-C$_6$-C$_7$-C$_8$ (18)
43(<1)	a" / τ C-CH$_3$ Ph (84); γ C$_{13}$-C$_6$-C$_8$-C$_7$ (11)

[a] Band intensities and shape: vs = very strong; s = strong; m = medium; w = weak; vw = very weak, sh: shoulder, br: broad. [b] In parenthesis computed IR intensities in Km/mol are given. [c] ν: stretching (subscripts "*s*" and "*as*" refer to symmetric and antisymmetric modes, respectively), δ: deformation, γ:out of plane deformation modes, ρ: rocking mode.

For compound **2**, vibrations of the 2*H*-chromen-2-thione ring give rise to medium intensity absorptions at 1257 and 1150 cm^{-1} assigned to coupled symmetric (ν$_s$COC) and antisymmetric (ν$_{as}$COC) motions of the C9–O–C1 internal coordinate, respectively. As reported by Burdzinski et al. for the thiocoumarin molecule, the C=S stretching coordinate is distributed over many normal modes without a normal mode dominantly localized on the the C=S stretch.[47] The same is valid for compound **2**: the potential energy distribution analysis suggest individual contributions of the C=S stretching coordinate to the frequencies (with a' symmetry) at 384(60%), 635(26%), 750(45%) and 1311(19%) cm^{-1} observed in both infrared and/or Raman spectra (see Table 4). The high intensity of the 384 and 635 cm^{-1} signals observed in the Raman spectrum is in line with this feature, since it is expected that the high polarizability of the C=S bond originates an intense Raman effect.

Finally, the νC=C stretching modes of the bencene system originate a series of intense absorptions at 1623, 1603 and 1537 cm^{-1}, the last two bands with strong counterparts in the Raman spectrum of compound **2** at 1596 and 1537 cm^{-1}, respectively.

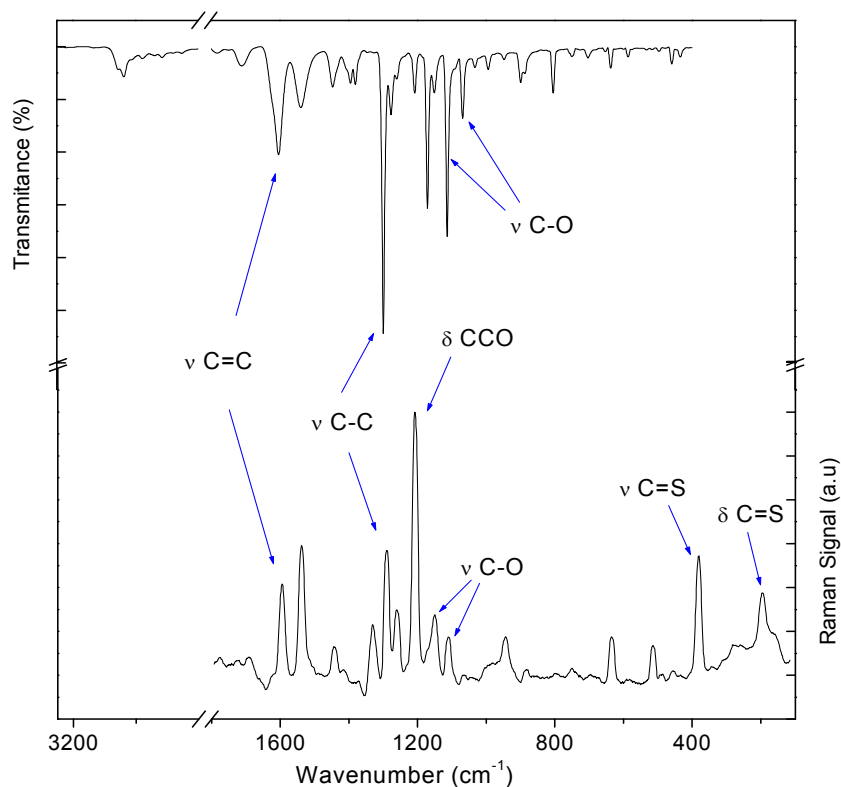**New Journal of Chemistry Accepted Manuscript**

Figure 6. FT-Raman and FTIR spectra for compound **2** in the solid phase.

Table 4. FTIR and Raman experimental data for compound **2**, together with the computed B3LYP/6-311++G(d,p) values and tentative normal mode assignment.

Experimental		Calculated [b]	Assignment [c] / % PED
IR [a]	Raman		
3132$_{vw}$		3210(1)	a'/ν CH (99)
3056$_m$		3193(7)	a'/ ν CH (100)
		3191(4)	a'/ ν CH (95)
3038$_m$		3168(8)	a'/ ν$_{as}$ CH (88)
3011$_w$		3121(15)	a' / ν$_{as}$ CH$_3$-Py (100)
3978$_w$		3112(13)	a' / ν$_{as}$ CH$_3$-Ph (99)
2939$_w$		3077(12)	a"/ν$_{as}$ CH$_3$-Ph (100)
		3075(9)	a"/ν$_{as}$ CH$_3$-Py (100)
2915$_w$		3028(25)	a'/ ν$_s$ CH$_3$-Ph (99)
		3027(16)	a'/ ν$_s$ CH$_3$-Py (100)
1623$_s$		1659(65)	a'/ ν CC (60) ring Ph; ν CC ring Py (40)
1603$_s$	1596$_s$	1638(216)	a' / ν CC Ph (63); ν CC Py (37)
1537$_s$	1537$_s$	1576(105)	a' / ν CC Ph (52); ν CC Py (48)

23

		1537(1)	a' / δ CC (68); δ OC_9C_8 (32)
1446_m	1442_m	1494(21)	a' / $δ_{as}$ CH_3-Ph (66); $δ_{as}$ CH_3-Py (18)
		1491(29)	a' / $δ_{as}$ CH_3-Py (67); $δ_{as}$ CH_3-Py (15)
		1486(8)	a" / $δ_{as}$ CH_3-Ph (76); τ $HC_{13}C_7C_8$ (24)
		1482(10)	a" / $δ_{as}$ CH_3-Py (77); τ $HC_{12}C_4C_3$ (23)
		1442(8)	a' / ν CC ring Ph (44) ; δ CH (42)
1394_m		1420(34)	a' / $δ_s$ CH_3-Py (51); δ CH (25)
1380_m		1417(2)	a' / $δ_s$ CH_3-Py (90)
		1405(7)	a' / $δ_s$ CH_3-Py (10); δ CH (46); ρ HC_5C_6H (44)
	1337_m	1359(14)	a' / δ CC ring Ph (71); $δ_s$ CH_3-Ph (29)
1300_{vs}	1294_s	1311(237)	a' / ν CC (60); ν CS (19); δ CCO (20)
1273_m			a' / Ph- ring breathing
1257_m	1260_s	1269(5)	a' / $ν_s$ COC (44); δ ring Ph (22);
1207_m	1206_{vs}	1225(20)	a' / δ CCO (65); Ph- ring breathing (34)
1169_s	1165_w	1186(57)	a' / δ CH ring Ph (58); δ CH ring Py (42)
1150_m	1146_m	1167(92)	a' / $ν_{as}$ COC (39); δ CH ring Ph (27)
1112_{vs}	1108_m	1121(139)	a' / δ CC ring Ph (34); δ CCO (26)
1068_m	1065_{vw}	1082(93)	a' / $ν_{as}$ COC (44); ν CC (27); τ CH_3-C_4C (27)
1031		1060(3)	a" / ρ CH_3-Ph (24); τ C_{13}-C_7-CH_3 (76)
		1057(3)	a" / ρ CH_3-Py (24); τ C_{12}-C_4-CH_3 (76)
		1028(5)	a' / $δ_{as}$ C_{13}-H (26); τ C_7-C_8-CH3 (74)
992_w		1009(16)	a' / $δ_{as}$ C_{12}H (59); ν C_4C_{12} (21); δ $C_6C_5C_{10}$(20)
946_{vw}	940_w	967(1)	a" / ρ H-C_6-C_7-H (77)
		966(2)	a' / δ C-C ring Ph (44); τ H-C_{13}-C_7-C_8 (55)
		893(0.03)	a" / ρ H-C_3-C_2-C_{13} (72); ρ H-C_8-C_7-C_{13} (28)
		889(8)	a' / ν CC ring Py (58); ν CO (42)
		885(27)	a" / ρ H-C_{13}-C_7-C_8 (76); ρ H-C_3-C_4-C_{12} (24)
804_m		821(26)	a' / ρ H-C_5-C_6-H (77)
750_w	753vw	770(1)	a' / ν C-S (45); δ ring Ph (55)
725_{vw}		742(1)	a" / τ C_8-C_9-C_{10}-C_5 (51); τ O-C_9-C_{10}-C_4 (49)
702_w		709(2)	a' / δ ring Ph (49); δ COC (51)
636_m	635_m	650(6)	a' / νC=S (26); δ ring Ph (74)
		643(1)	a" / γ S-C-O-C (58); γ $C_{13}C_6C_8C_7$ (42)
585_m		588(5)	a" / γ C_7-C_6-C_8-C_{13} (58); γ S-C-O-C (42)
527_{vw}	521_m	532(0.1)	a" / τ C_8-C_8-C_{10}-C_5 (12); γ S-C-O-C (52); γ C_3-C_4-C_{10}-C_{12} (36)
		523(1)	a' / δ C_5-C_{10}-C_9 (45);δ O-C_9-C_8 (28); ν CH_3-Py (27)
497_{vw}	492_w	500(1)	a' / τ H-C_{13}-C_7-C_8 (83); ν CH_3-Py (18)
458_w		464(9)	a' / δ C_2-C_3-O (38); δ C_7-C_8-C_9 (36) ; ν CH_3-Ph (25);
435_w		445(7)	a" / γ O-C_{10}-C_8-C_9 (85); γ S-C-O-C (14)
	384_s	386(5)	a' / νC=S (60); δ C-O-C (40)
		337(0.07)	a' / ρ C-CH_3 -Ph (52); ρ C-CH_3 Py (48)
		274(0.2)	a" / τ C_4-C_3-C_2-O (62); τ ring Ph (48)
		258(1)	a' / δ C_2-C_3-C_4 (73); δ C_5-C_6-C_7 (27)
		247(0.0004)	a" / γ CH_3-Ph(83); γ O-C_{10}-C_8-C_9 (16)
		198(1)	a" / ρ CH_3 ring Py (84); τ C_3-C_2-O-C_9 (16)
	197_m	190(0.4)	a' / δ CS (59); δ C-H ring Ph (41)
		158(0.001)	a" / τ H-C_{12}-C_4-C_3 (36); τ C_3-C_2-O-C_9 (64)
		98(2)	a" / τ C_2-O-C_9-C_{10} (85); τ C_3-C_2-O-C_9 (15)
		73(0.2)	a' / τ S-C-O-C (12); τ ring Ph (87)
		34(0.2)	a" / ρ H-C_{13}-H (95)

[a] Band intensities and shape: vs = very strong; s = strong; m = medium; w = weak; vw = very weak, sh: shoulder, br: broad. [b] In parenthesis computed IR intensities in Km/mol are given. [c] ν: stretching (subscripts s and as refer to symmetric and antisymmetric modes, respectively), δ: deformation, γ:out of plane deformation modes, ρ: rocking mode.

3.4- Outermost electronic properties and UV-Visible spectra

Figure 7 shows the experimental and calculated UV/Vis spectra in the 200–800 nm range for both compounds isolated in a vaccum and dissolved in CH_2Cl_2. The spectra are evaluated from the calculated TD-B3LYP/6-311++G(d,p) vertical electronic transitions energies and oscillator strengths between the initial and final states and the assigned transitions with major contributions for **1** and **2** are shown in Table 5. Moreover, the character of the orbitals involved in the main electronic transitions, together with their energy (in eV), for compounds **1** and **2** are shown in Figure 8. Similar vertical transition energies are found when the vacuum isolated and solvated molecules are compared. The most salient difference being observed for the HOMO-LUMO transition for compound **2**, which shows a notable bathochromic shift (positive solvatochromism from 488.3 nm (vacuum) to 436.6 nm (CH_2Cl_2), the last value in good agreement with the experimental spectrum (see below).

For compound **1**, two absorption bands are observed at 315 and 276 nm. The lower energy transition corresponds to the HOMO→ LUMO (74%) transition. The second band at 276 nm is associated with two very close transitions computed at 274 and 271 nm associated with HOMO–2→ LUMO (92%) and HOMO–1→ LUMO (70%) for the compound **1.** This assignment is in agreement with recently reported spectra of related coumarins [44] and chromones.[42, 48]

The UV-Vis spectrum for compound **2** shows intense and broad band centered at 377 nm, with a shoulder clearly observed at 394 nm and the non-symmetric tail toward the high-wavenumber region suggest the presence of a absorption occurring at ca. 420 nm. A less intense absorption is defined at 311 nm and a band at 270 nm occurs in the UV region of the spectrum. With the help of quantum chemical calculations, the shoulder at 420 nm was assigned to the

New Journal of Chemistry Accepted Manuscript

formally forbidden HOMO→ LUMO (92%) transition. The most intense bands at 377 and 394 nm were associated to the HOMO–1→ LUMO (74%) transition, whereas the 311 nm band is well reproduced by the calculations as originated by the HOMO→ LUMO+1 (93%) electron promotion. Finally, the band at 270 nm is associated to the HOMO–2→ LUMO (70%) transition.

When the characters of frontier molecular orbitals are analysed, it becomes apparent that differences in the electronic properties of the 1-benzopyran-2-one and 1-benzopyran-2-thione groups occur. Thus, for compound **1**, the HOMO corresponds to a π bonding system localized over phenyl moiety with contributions of the p-type lone pair orbital of oxygen with a'' symmetry. On the other hand, for compound **2**, the HOMO displays a' symmetry and is associated with purely p-type lone pair orbital located at the sulfur atom. The HOMO–1 corresponds to a π bonding system localized over 1-benzopyran moiety for **1**, while the contribution of the a'' sulfur lone pair orbital is observed for compound **2**. For both compounds, the LUMOs have a'' symmetry associated with π antibonding system delocalized over the 1-benzopyran group. As a result, for compound **2** the HOMO–LUMO is forbidden and the oscillator strength is very low for the HOMO→ LUMO+1 transitions.

The formal change of oxygen atom by the large and more polarizable sulfur atom in **1** and **2**, respectively, affects the UV-Vis spectra of these analogues, not merely by shifting the whole absorptions of compound **2** to lower energies, as expected,[49] but also changing the electronic transitions.

Figure 7. Experimental (blue) and computed (red) UV-Vis spectra of compounds **1** (left, 7.8 x 10⁻⁶ M in CH_2Cl_2) and **2** (right, 4.7 x 10⁻⁶ M in CH_2Cl_2).
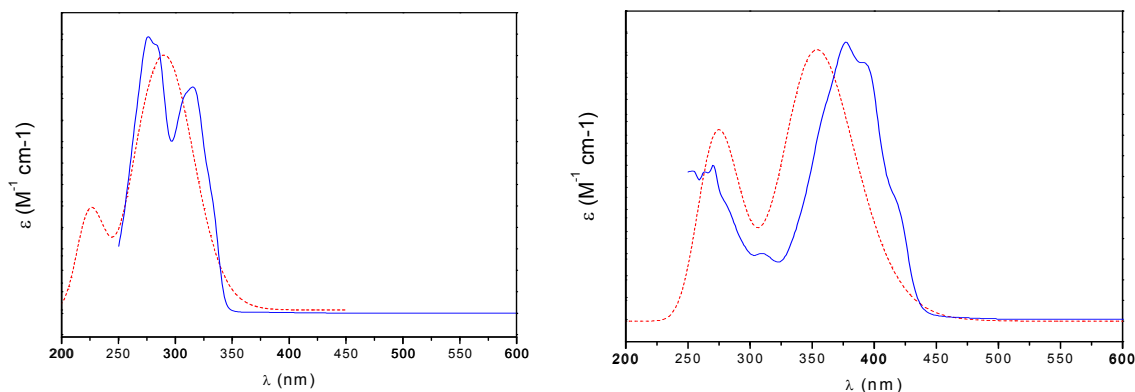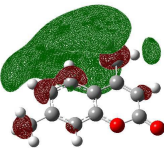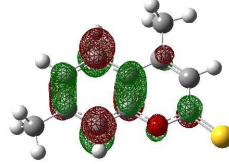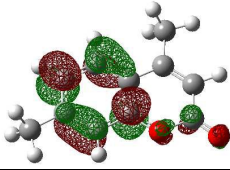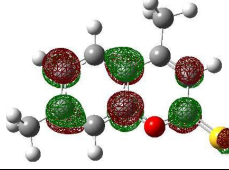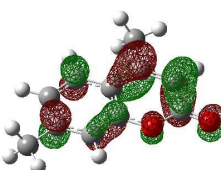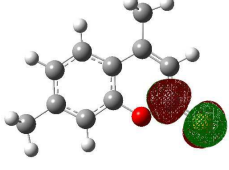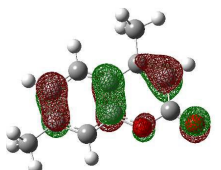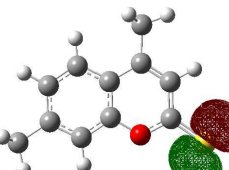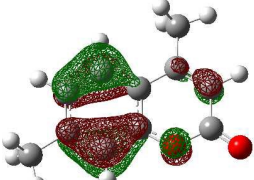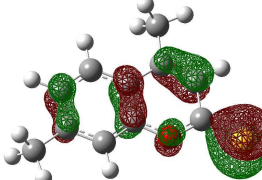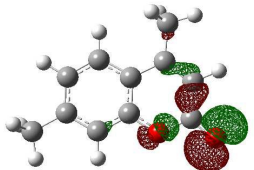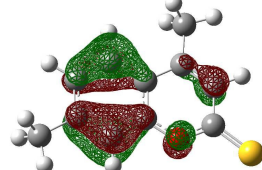
Table 5. Experimental and calculated absorption wavelength (nm) and oscillator strengths of the most significant excited states for compounds **1** and **2**.

Wavelength (nm)		Oscillator strength [a]	Assignment
Experimental	**Calculated** [a]		
Compound **1**			
315	299.2/302.3	0.179/0.301	HOMO→ LUMO (74%)
			HOMO–1→ LUMO (9%)
			HOMO–1→ LUMO+1 (5%)
276	274.0/280.7	0.000/0.000	HOMO–2→ LUMO (92%)
			HOMO–2→ LUMO+3 (3%)
	271.5/267.4	0.122/0.138	HOMO–1→ LUMO (70%)
			HOMO→ LUMO (7%)
			HOMO→ LUMO+1 (14%)
	234.0/233.3	0.037/0.041	HOMO→ LUMO+1 (47%)
			HOMO–1→ LUMO+1 (14%)
			HOMO–1→ LUMO+3 (14%)
			HOMO–1→ LUMO+3 (9%)
			HOMO–1→ LUMO (8%)
Compound **2**			
420 sh	488.3/436.6	0.000/0.001	HOMO→LUMO (92%)
394 sh	354.2/363.6	0.324/0.537	HOMO–1→LUMO (74%)
377			HOMO–1→LUMO+1 (4%)
311	306.3/306.9	0.001/0.028	HOMO→LUMO+1 (93%)
			HOMO→LUMO+2 (3%)
270	292.6/276.0	0.003/0.001	HOMO–2→LUMO (70%)
			HOMO–1→LUMO+1 (18%)
			HOMO–1→LUMO+2 (5%)

[a] TD-B3LYP/6-311++G(d,p), Vacuum/CH_2Cl_2 parameters.

**Figure 8.** Plots of the frontier molecular orbitals calculated for compounds **1** (left) and **2** (right).

Computed energies are also given.

Type	Compound 1	Compound 2
LUMO +2		
	-0.462 eV	0.381eV
LUMO +1		
	-0.816 eV	0.082 eV
LUMO		
	-2.014 eV	-1.524 eV
HOMO		
	-6.585 eV	-5.469 eV
HOMO –1		
	-7.183 eV	-7.320 eV
HOMO –2		
	-7.701 eV	-7.456 eV

3.5- NBO Analysis

To further study the influence of the heteroatom in the electronic delocalization over the 1-benzopyran-2-one/thione fragment (see Scheme 4), NBO population analysis has been performed.[48] The results for both compounds indicate the presence of pure p-type lone pair orbitals with a'' symmetry [$lp_\pi(O)$] formally centered at the endocyclic oxygen atom. The $lp_\pi(O)$ for compounds **1** and **2** display low electron occupancy, 1.734 and 1.720 **e**, indicating the electron-donating capacity for these orbitals. Delocalizing interactions evaluated by a second-order perturbation approach reveals that the $lp_\pi(O)$ lone pair orbital contributes to a strong resonance interactions with both adjacent $\pi^*(C=O)$ and $\pi^*(C=S)$ antibonding orbitals, amounting up to 31.66 y 39.53 kcal/mol, for **1** and **2**, respectively. Similar interaction values have been reported recently by Arivazhagan et al. for the related species 3-methyl coumarine.[50] Concomitantly, the electron occupancy of the $\pi^*(C=O)$ (0.276 **e**) is low than that of the $\pi^*(C=S)$ (0.386 **e**) acceptor. In qualitative agreement with these delocalizing electronic interaction values, the O–C bond length in compound **2** [1.361(3)] is shorter than that of compound **1** [1.378(2)].

Scheme 4. Resonance structures for the 1-benzopyran-2-one/thione (X= O/S) fragment
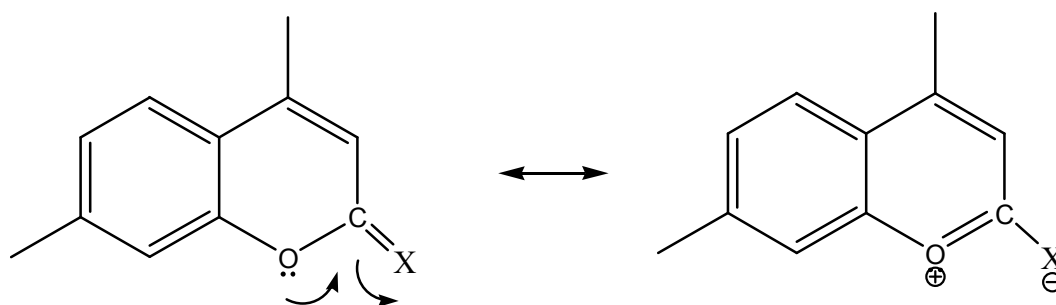
4- Conclusion

In summary, we have extended the use of Lawesson's reagent for synthetizing 4,7-dimethyl-2*H*-chromen-2-thione (**2**). The structural and spectroscopic (vibrational and electronic) properties have been studied and compared with the oxygen analogue, i.e. 4,7-dimethyl-2*H*-chromen-2-one (**1**), allowing for a clear determination of the effect produced by the formal change of the oxygen atom by the large and more polarizable sulfur atom in the 1-benzopyran-2-one/thione moiety. These results are of interest for both, coumarin and chromone compounds.

5- Electronic Supplementary Information

Atomic coordinates and equivalent isotropic displacement parameters, geometrical parameters, anisotropic displacement parameters and hydrogen coordinates derived from the X-ray diffraction analysis are given in Tables S1-S4. GC-MS spectra for compounds **1** and **2** are given in Figures S1 and S2, respectively.The ^{13}C and ^{1}H and 2D (HSQC and HMBC) NMR spectra for compound **2** are given in Figures S4-S7.

6- Acknowledgements

7- References

1. C. Kontogiorgis, A. Detsi and D. Hadjipavlou-Litina, *Exp. Opin. Therap. Pat.*, 2012, **22**, 437-454.
2. W. H. Perkin, *J. Chem. Soc.*, 1868, **21**, 53-63.
3. R. H. Vekariya and H. D. Patel, *Synt. Comm.*, 2014, **44**, 2756-2788.
4. F. G. Medina, J. G. Marrero, M. Macias-Alonso, M. C. Gonzalez, I. Cordova-Guerrero, A. G. Teissier Garcia and S. Osegueda-Robles, *Nat. Prod. Rep.*, 2015, **32**, 1472-1507.
5. M. Alipour, M. Khoobi, A. Moradi, H. Nadri, F. Homayouni Moghadam, S. Emami, Z. Hasanpour, A. Foroumadi and A. Shafiee, *Eur. J. Med. Chem.*, 2014, **82**, 536-544.
6. P. O. Patil, S. B. Bari, S. D. Firke, P. K. Deshmukh, S. T. Donda and D. A. Patil, *Bioorg. Med. Chem.*, 2013, **21**, 2434-2450.
7. M. A. Musa, J. S. Cooperwood and M. O. F. Khan, *Curr. Med. Chem.*, 2008, **15**, 2664-2679.
8. D. Lafitte, V. Lamour, P. O. Tsvetkov, A. A. Makarov, M. Klich, P. Deprez, D. Moras, C. Briand and R. Gilli, *Biochemistry*, 2002, **41**, 7217-7223.
9. A. Saeed, S. Ashraf, U. Flörke, Z. Y. Delgado Espinoza, M. F. Erben and H. Pérez, *J. Mol. Struct.*, 2016, **1111**, 76-83.
10. K. Wang, Z. Liu, R. Guan, D. Cao, H. Chen, Y. Shan, Q. Wu and Y. Xu, *Spectrochim. Acta*, 2015, **144A**, 235-242.
11. F. Pérez-Cruz, S. Vazquez-Rodriguez, M. J. Matos, A. Herrera-Morales, F. A. Villamena, A. Das, B. Gopalakrishnan, C. Olea-Azar, L. Santana and E. Uriarte, *J. Med. Chem.*, 2013, **56**, 6136-6145.
12. A. Saeed, S. Zaib, S. Ashraf, J. Iftikhar, M. Muddassar, K. Y. J. Zhang and J. Iqbal, *Bioorg. Chem.*, 2015, **63**, 58-63.
13. S. Scheibye, J. Kristensen and S. O. Lawesson, *Tetrahedron*, 1979, **35**, 1339-1343.
14. J. Voss, R. Edler and G. Adiwidjaja, *Phosphorus, Sulfur, and Silicon Relat. Elem.*, 2007, **182**, 1893-1905.
15. A. Levai and J. Jekő, *J. Heterocyclic Chem.*, 2005, **42**, 739-742.
16. a) P. Munshi and T. N. Guru Row, *Acta Crystallogr.*, 2001, **E57**, o1175-o1176. b) P. Munshi and T.N. Guru Row, Acta Crystallogr., 2002, **B58**, 1011-1017.
17. M. G. Choi, Y. H. Kim, J. E. Namgoong and S.-K. Chang, *Chem. Comm.*, 2009, 3560-3562.
18. J. E. Park, M. G. Choi and S.-K. Chang, *Inorg. Chem.*, 2012, **51**, 2880-2884.
19. S. K. Seth, D. Sarkar, A. D. Jana and T. Kar, *Cryst. Growth Des.*, 2011, **11**, 4837-4849.
20. A. E. Reed, L. A. Curtiss and F. Weinhold, *Chem. Rev.*, 1988, **88**, 899-926.
21. T. J. Curphey, *J. Org. Chem.*, 2002, **67**, 6461-6473.
22. A. Saeed and Z. Ashraf, *J. Heterocyclic Chem.*, 2008, **45**, 679-682.
23. CrysAlisPro, *Oxford Diffraction Ltd., version 1.171.33.48 (release 15-09-2009 CrysAlis171.NET)*.
24. G. Sheldrick, *Acta Crystallogr.*, 2008, **A64**, 112-122.
25. M. J. Frisch, G. W. Trucks, H. B. Schlegel, G. E. Scuseria, M. A. Robb, J. R. Cheeseman, J. A. Montgomery Jr., T. Vreven, K. N. Kudin, J. C. Burant, J. M. Millam, S. S. Iyengar, J. Tomasi, V. Barone, B. Mennucci, M. Cossi, G. Scalmani, N. Rega, G. A. Petersson, H. Nakatsuji, M. Hada, M. Ehara, K. Toyota, R. Fukuda, J. Hasegawa, M. Ishida, T. Nakajima, Y. Honda, O. Kitao, H. Nakai, M. Klene, X. Li, J. E. Knox, H. P. Hratchian, J. B. Cross, C. Adamo, J. Jaramillo, R. Gomperts, R. E. Stratmann, O. Yazyev, A. J. Austin, R. Cammi, C. Pomelli, J. W. Ochterski, P. Y. Ayala, K. Morokuma, G. A. Voth, P.

Salvador, J. J. Dannenberg, V. G. Zakrzewski, S. Dapprich, A. D. Daniels, M. C. Strain, O. Farkas, D. K. Malick, A. D. Rabuck, K. Raghavachari, J. B. Foresman, J. V. Ortiz, Q. Cui, A. G. Baboul, S. Clifford, J. Cioslowski, B. B. Stefanov, G. Liu, A. Liashenko, P. Piskorz, I. Komaromi, R. L. Martin, D. J. Fox, T. Keith, M. A. Al-Laham, C. Y. Peng, A. Nanayakkara, M. Challacombe, P. M. W. Gill, B. Johnson, W. Chen, M. W. Wong, C. Gonzalez and J. A. Pople, Gaussian, Inc., Pittsburgh PA, 2003.

26. M. J. Frisch, J. A. Pople and J. S. Binkley, *J. Chem. Phys.*, 1984, **80**, 3265-3269.
27. M. H. Jamróz, *Spectrochim. Acta*, 2013, **114A**, 220-230.
28. M. H. Jamróz, *Vibrational Energy Distribution Analysis VEDA 4*, Warsaw, 2004.
29. M. E. Casida, C. Jamorski, K. C. Casida and D. R. Salahub, *J. Chem. Phys.*, 1998, **108**, 4439-4449.
30. V. Barone and M. Cossi, *J. Phys. Chem. A*, 1998, **102**, 1995-2001.
31. J. J. McKinnon, D. Jayatilaka and M. A. Spackman, *Chem. Comm.*, 2007, 3814-3816.
32. M. A. Spackman and D. Jayatilaka, *CrystEngComm*, 2009, **11**, 19-32.
33. M. A. Spackman, *Phys. Scr.*, 2013, **87**, 048103.
34. J. J. McKinnon, M. A. Spackman and A. S. Mitchell, *Acta Crystallogr.*, 2004, **60B**, 627-668.
35. S. K. Wolff, D. J. Grimwood, J. J. McKinnon, M. J. Turner, D. Jayatilaka and M. A. Spackman, University of Western Australia, 2012.
36. Q. N. Porter, *Mass Spectrometry of Heterocyclic Compounds*, John Wiley & Sons, New York, 1985.
37. J. P. Kutney, G. Engendorf, T. Inaba and D. L. Dreyer, *Org. Mass Spectrom.*, 1971, **5**, 249-263.
38. J. L. Farrugia, *J. Appl. Crystallogr.*, 1997, **30**, 565.
39. L. R. Gomes, J. N. Low, F. Cagide, D. Chavarria and F. Borges, *Acta Crystallogr.*, 2015, **E71**, 547-554.
40. A. Saeed, A. Ibrar, M. Arshad and M. Bolte, *Acta Crystallogr.*, 2012, **E68**, o3024.
41. M. Malecka and E. Budzisz, *CrystEngComm*, 2014, **16**, 6654-6663.
42. C. D. Alcívar León, G. A. Echeverría, O. E. Piro, S. E. Ulic, J. L. Jios, M. Burgos Paci and G. A. Argüello, *Chem. Phys.*, 2016, **472**, 142-155.
43. L. P. Avendaño Jiménez, G. A. Echeverría, O. E. Piro, S. E. Ulic and J. L. Jios, *J. Phys. Chem. A*, 2013, **117**, 2169-2180.
44. P. Koparir, K. Sarac, C. Orek and M. Koparir, *J. Mol. Struct.*, 2016, **1123**, 407-415.
45. Y. Sert, K. B. Puttaraju, S. Keskinoğlu, K. Shivashankar and F. Ucun, *J. Mol. Struct.*, 2015, **1079**, 194-202.
46. N. Kuş, S. Breda, I. Reva, E. Tasal, C. Ogretir and R. Fausto, *Photochem. Photobiol.*, 2007, **83**, 1541-1542.
47. G. Burdzinski, G. Buntinx, O. Poizat and C. Lapouge, *Journal of Molecular Structure,* 2005, **735-736**, 115-122.
48. K. Gokula Krishnan, R. Sivakumar, V. Thanikachalam, H. Saleem and M. Arockia doss, *Spectrochim. Acta*, 2015, **144A**, 29-42.
49. A. Saeed, S. Ashraf, J. M. White, D. B. Soria, C. A. Franca and M. F. Erben, *Spectrochim. Acta*, 2015, **150A**, 409-418.
50. M. Arivazhagan, R. Kavitha and V. P. Subhasini, *Spectrochim. Acta*, 2014, **130A**, 502-515.1

The importance of being polarizable

Structural and spectroscopic properties of the 1-benzopyran-2-one/thione moiety